

Full paper

Three-dimensional ultraflexible triboelectric nanogenerator made by 3D printing

Baodong Chen^{a,b,1}, Wei Tang^{a,b,1}, Tao Jiang^{a,b,1}, Laipan Zhu^{a,b}, Xiangyu Chen^{a,b}, Chuan He^{a,b}, Liang Xu^{a,b}, Hengyu Guo^{a,b}, Pei Lin^{a,b}, Ding Li^{a,b}, Jiajia Shao^{a,b}, Zhong Lin Wang^{a,b,c,*}

^a Beijing Institute of Nanoenergy and Nanosystems, Chinese Academy of Sciences, Beijing 100083, PR China

^b College of Nanoscience and Technology, University of Chinese Academy of Sciences, Beijing 100049, PR China

^c School of Material Science and Engineering, Georgia Institute of Technology, Atlanta, GA 30332-0245, USA

ARTICLE INFO

Keywords:

Ultraflexible triboelectric nanogenerator
3D printing
Self-powered source
Energy harvesting

ABSTRACT

As the fast developments of wearable devices, artificial intelligences and Internet of Things, it is important to explore revolutionary approach and fabrication method for providing flexible and sustainable power sources. We report here a practical, ultraflexible and three-dimensional TENG (3D–TENG) that is capable of driving conventional electronics by harvesting biomechanical energy. Such TENG is made for the first time by the unique additive manufacturing technology—hybrid UV 3D printing. The TENG is made up of printed composite resin parts and ionic hydrogel as the electrification layer and electrode. A sustainable and decent output of 10.98 W/m³ (P_v , peak power per unit volume) and 0.65 mC/m³ (ρ_{sc} , transferred charge per unit volume) are produced under a low triggering frequency of ~ 1.3 Hz, which is attributed to the Maxwell's displacement current. Meanwhile, a self-powered SOS flickering and buzzing distress signal system, and smart lighting shoes are successfully demonstrated, as well as self-powered portable systems of a temperature sensor or a smart watch. Our work provides new opportunities for constructing multifunctional self-powered systems toward the applications in realistic environments.

1. Introduction

The rapid growth of flexible and multifunctional electronics imposes the challenges on portable power sources that feature in high flexibility. Self-powered Nanosystems [1,2] and stretchable/transparent actuators [3,4] have been recently demonstrated, but the power sources lack high flexibility and high-density integration. Since the soft and wearable electronics are widely integrated in clothes and shoes, and some of them are also attached on forced parts of human body [5,6], their power sources are supposed to be highly flexible, shape-adaptive, and capable of driving applications ranging from integrated circuits [7,8] to soft sensor [9–11], etc. Because of the conversion mechanism, conventional electromagnetic generators and silicon-based solar cells are not able to achieve high flexibility. On the contrary, the recently reported triboelectric nanogenerator (TENG) can be fabricated to be flexible. It can convert mechanical energy into electricity based on the triboelectrification effect coupled with the electrostatic induction [12–16]. It has the advantages of simple structure, vast material choices, and low cost [17–26].

Here, we report a practical, ultraflexible three-dimensional TENG (3D–TENG), which can drive or charge common electronics through harvesting energy from human motions. More importantly, this device is fabricated by a unique additive manufacturing technology—hybrid 3D printing technique. Different from previous TENGs with dielectric films as the triboelectric materials, such ultraflexible 3D–TENG uses printed composite resin parts (with a high printing precision of 1 μm) and ionic hydrogel as the electrification layer and electrode. It can be applied for biomechanical energy harvesting, such as human motions (usually less than 3 Hz). It was found that under a low frequency of around 1.3 Hz, an instantaneous peak power density of 10.98 W/m³ and a transferred charge density of 0.65 mC/m³ were achieved. Additionally, self-powered wearable devices such as LEDs flickering and buzzing SOS distress systems, and smart LEDs lighting shoes are successfully demonstrated.

* Corresponding author at: Beijing Institute of Nanoenergy and Nanosystems, Chinese Academy of Sciences, Beijing 100083, China.

E-mail address: zlwang@gatech.edu (Z.L. Wang).

¹ These authors contributed equally to this work.

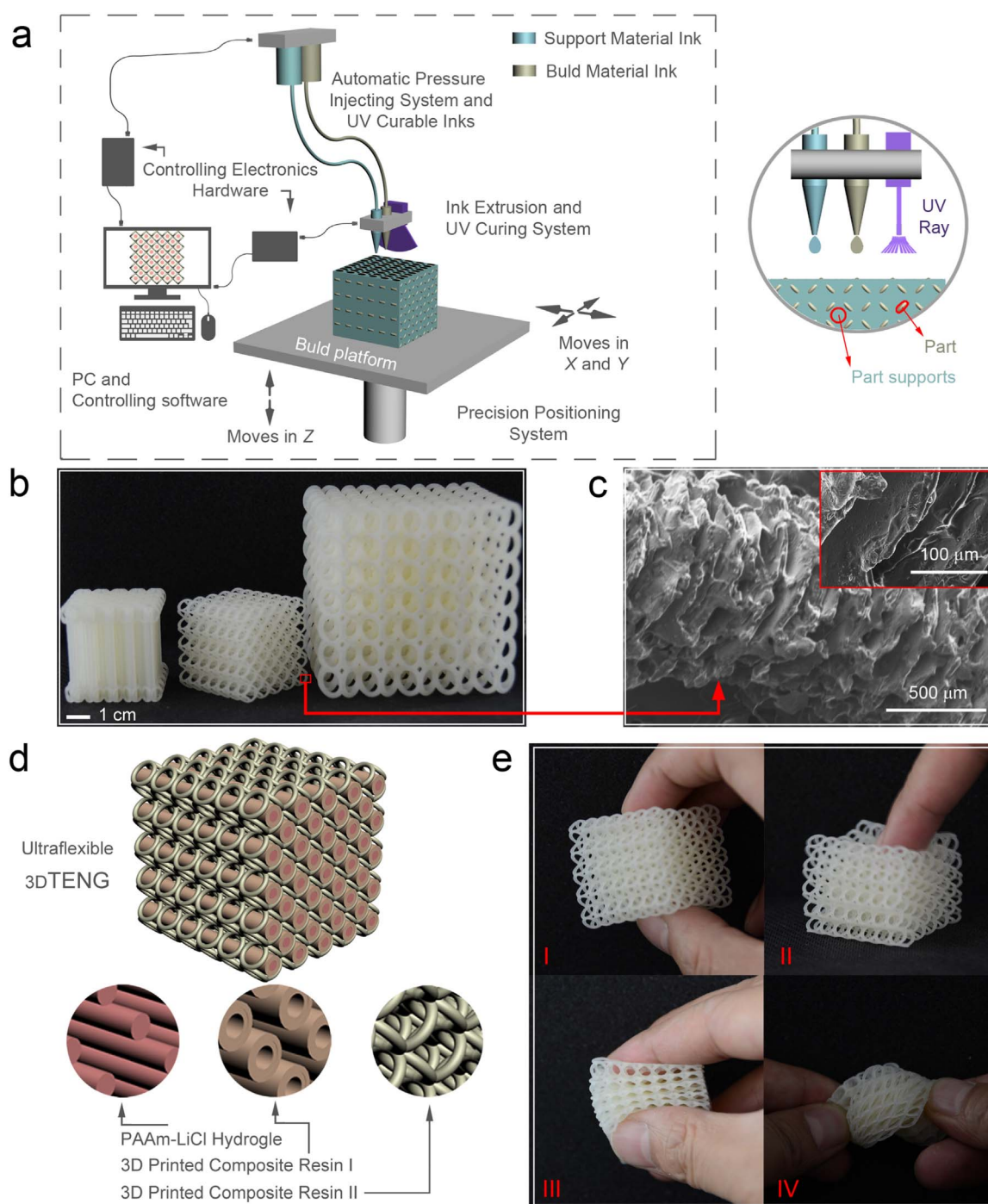


Fig. 1. Structure of the ultraflexible 3D-TENG and its fabrication process. **a**, Overall schematic of the hybrid 3D printing system used in this study. **b**, Digital image of the final 3D printed ultraflexible parts. **c**, SEM images of the ultraflexible part. **d**, The design of ultraflexible 3D-TENG. **e**, Ultraflexible test of the ultraflexible 3D printed parts.

2. Experimental section

2.1. The structure and fabrication process of the ultraflexible 3D-TENG

Printing was performed using an UV curing 3D printer [27,28] comprised of automatic pressure injecting device, ink extrusion and UV curing system, precision positioning platform, PC and hardware/software control system, as schematically illustrated in Fig. 1a. The schematic of the hybrid 3D printing system plan is shown in Supplementary Fig. 1. This is a new method of hybrid 3D printing for producing ultraflexible parts, in which the liquid photopolymer resins and support materials are directly printed by using a single manufacturing process

within an integrated platform [29–31]. Printed parts with additive internal supporting structure are intended to keep high accuracy of ultraflexible printed parts and shape unchanged, and then the internal supporting structure is removed by corrosive reagents without affecting other parts (Supplementary Fig. 2). Finally, the ultraflexible parts are obtained to act as the electrification materials of TENGs (Fig. 1b). Supplementary Fig. 3 demonstrates our printing capabilities of complex 3D-structure designs by comparing the final 3D printed ultraflexible parts. The SEM analysis about the micro-morphology of the ultraflexible printed parts shows that the UV curing forms a layer-upon-layer structure along the printing direction as the object is fully realized (Fig. 1c). In this approach, digital light processing UV curing system

was used to partially set the extruded resins and provide the high accuracy (i.e., $< 10 \mu\text{m}$, Supplementary Fig. 4) allowing a designed performance of ultraflexible part relevant to application requirements. The ultraflexible 3D-TENG uses printed resin parts and ionic hydrogel as the electrification material and electrode, respectively, which together make up one columnar array of triboelectric interfaces. Its structure and assembly process are schematically illustrated in Fig. 1d and Supplementary Fig. 5 and the ultraflexibility test are presented in Fig. 1e and Supplementary Video 1.

Supplementary material related to this article can be found online at <http://dx.doi.org/10.1016/j.nanoen.2017.12.049>

2.2. Methods and materials

Hybrid 3D printing system is comprised of automatic pressure injecting system, ink extrusion and UV curing system, precision positioning platform, PC and hardware/software control system (Fig. 1a and Supplementary Fig. 1a). The UV curing ink (liquid photopolymer

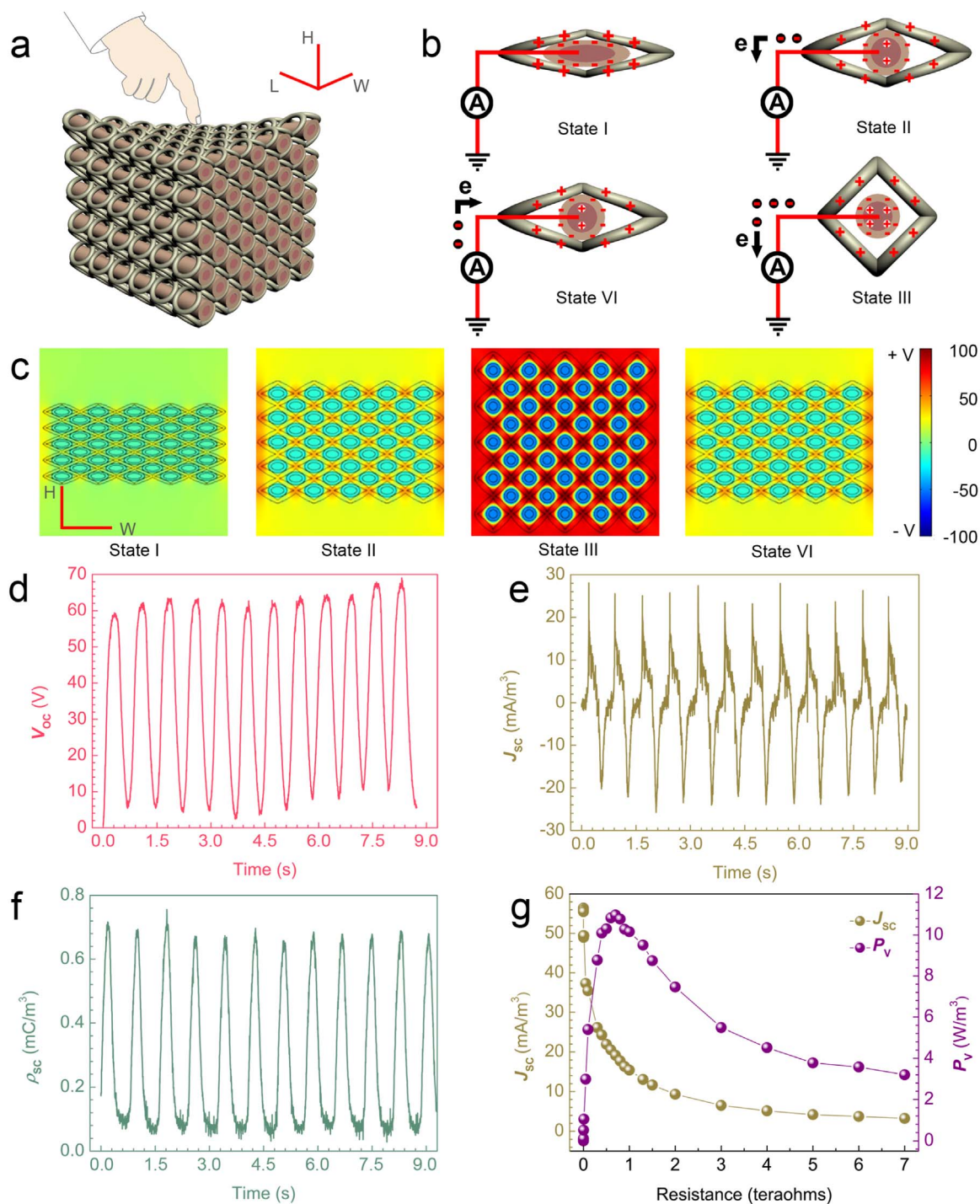


Fig. 2. Working principles of the ultraflexible 3D-TENG and its output performance. a, Diagrammatic drawing showing the deformational process of the ultraflexible 3D-TENG. b, Schematic diagram showing the working principles of the ultraflexible 3D-TENG. c, The numerically calculated electrical potentials distribution of the ultraflexible 3D-TENG. d, Output open circuit voltages (V_{oc}), volume current density (J_{sc}) (e) and transfer volume charge density (ρ_{sc}) (f) of the ultraflexible 3D-TENG under low frequency of ~ 1.3 Hz from human motions. g, Characteristics of the J_{sc} and power density (P_v) with the external loading resistance.

resin) was prepared based on acrylate oligomer (~ 70 wt%), acroleic acid (~ 25 wt%), photoinitiator (~ 2 wt%), reactive diluents and additives (~ 3 wt%). The composite resins I and II were prepared by mixing the UV curing ink base and different masses of acrylonitrile butadiene styrene powder, 1:1.5 and 1:2 by weight, and then 3D printing was carried out. The PAAM-LiCl hydrogel was prepared according to the method reported previously. Briefly, acrylamide powder was added into LiCl (8 M) aqueous solution. Subsequently, N, N'-methylenebisacrylamide, ammonium persulfate, and N, N', N'-tetramethylethylenediamine (Sigma-Aldrich) were dissolved in the solution consecutively. The solution was then transferred into a cylindrical array of glass mold and treated in an oven at 45 °C for 3 h to form the PAAM-LiCl hydrogel (Supplementary Fig. 1d).

The fabrication process of the ultraflexible 3D-TENG includes the developing of ultraflexible 3D printer, material preparation (composite resins), 3D modeling (3D MAX), printing setup (for instance, a size of 3.5 cm × 3.5 cm × 3.5 cm, 3D printing of composite resin II part will

need 180 g of composite resin II and 345 g of Supporting material and 10 min of build times), 3D printing and integration assembly. According to the fabrication process as shown in Supplementary Fig. 1d, the ultraflexible 3D-TENG was successful assembled. Finally, the copper wire was attached to the hydrogel for electrical connection. The morphology of the nanostructured rubber surface was characterized by a field emission scanning electron microscope (Hitachi SU8020). The electrical output signals (voltage, charge, and current) of the ultraflexible 3D-TENGs were measured by a programmable electrometer (Keithley, part no. 6517B) and data acquisition card. A linear motor (LinMot E1100) was used to form alternative motions and drive the device to contact and separate for quantified measurement. In addition, the data were collected and recorded by computer-controlled measurement software written in LabVIEW.

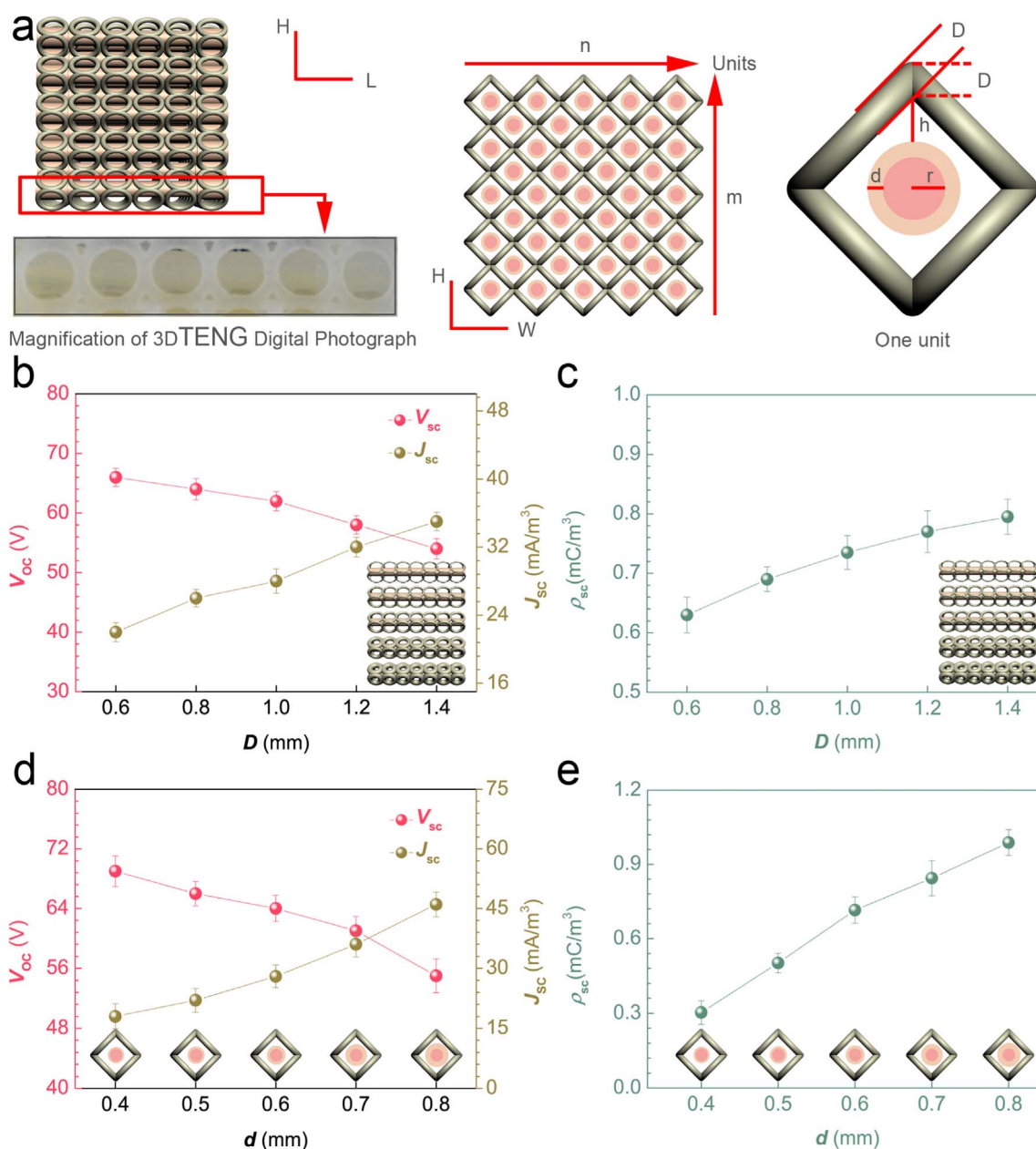


Fig. 3. The influence of structure parameters on the electrical output performances. **a**, Diagrammatic drawing showing the structure and parameters of the ultraflexible 3D-TENG. **b**, The V_{oc} , J_{sc} and ρ_{sc} (c) of the ultraflexible 3D-TENG with different D (mm). **d**, The V_{oc} , J_{sc} and ρ_{sc} (e) of the ultraflexible 3D-TENG with different d (mm).

3. Results and discussion

3.1. Electrical signal generation

The continuous operation of the ultraflexible 3D-TENG is based on compressive deformation and elastic recovery of the shape (Fig. 2a). A typical approach for harvesting the biomechanical energy is to employ the printed ultraflexible parts made of photopolymer resins as the triboelectrification layer and the ionic hydrogel as the electrode. The electrode is connected to the ground by a metal wire through the external load, and the TENG works in a single-electrode mode whose four

typical states are shown in Fig. 2b. Previous studies have shown the universality of contact electrification between any two different materials (different dielectric constants) [32–35], and here the printed resin I part and resin II part have different chemical components. When the two different resin materials were contacted with each other by external stress from biomechanical energy, the same amount of charges with opposite signs are generated on their surfaces (State I, fully compressed) due to their different surface electron affinities [36–38]. At this point the two opposite charges almost coincide, and no electrical potential difference exists between the two surfaces [39–42]. When the two surfaces are separating, the static charges on the surface of resin I

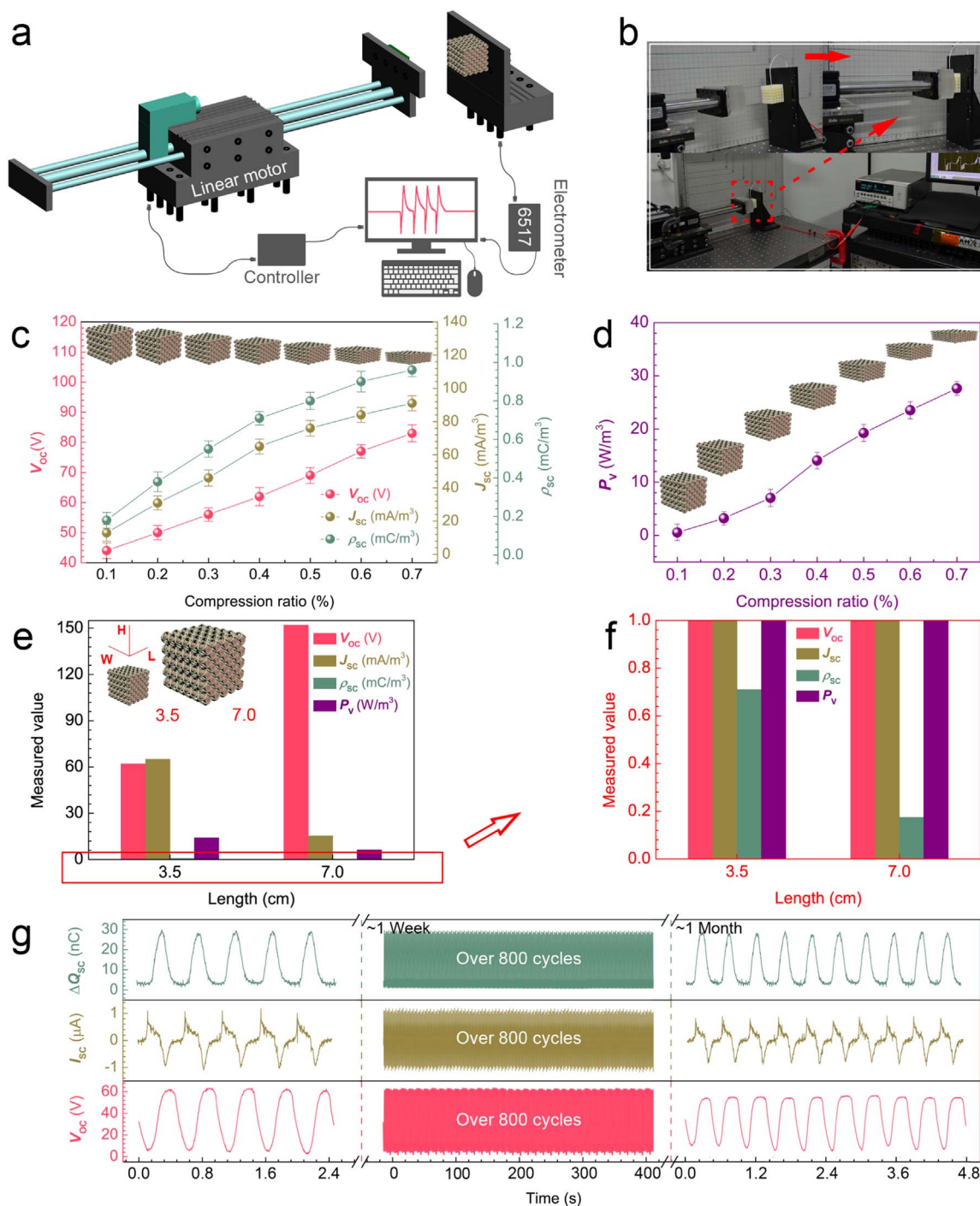


Fig. 4. The compression ratio, sizes and durability of the ultraflexible 3D-TENG. a, Working process of the ultraflexible 3D-TENG by a linear motor and digital images (b). c, The V_{oc} , J_{sc} and ρ_{sc} of the ultraflexible 3D-TENG with different compression ratio (%). d, The P_v of the ultraflexible 3D-TENG with different compression ratio (%). e, The V_{oc} , J_{sc} and ρ_{sc} and P_v of the ultraflexible 3D-TENG with different length (cm) and magnified view (f). g, The durability test of the ultraflexible 3D-TENG.

will induce the ion movement in the ionic hydrogel to balance the potential field, producing positive charges at the hydrogel interface (State II, recovery process). A negative electric potential difference will be established between the hydrogel electrode and ground, generating the current flow through the external circuits until the maximum separation (State III, fully recovered). When the resin II are compressed again to get close to the resin I, the whole process will be reversed and a reversed current flow occurs (State IV, compression process). By repeating the compression-recovery deformation for the ultraflexible 3D-

TENG, a periodic alternative current will be generated.

The electrical potential distributions for the ultraflexible 3D-TENG with four typical states are numerically calculated as shown in Fig. 2c. The simulation results show that as the distance between the resin I and resin II increases, the electrical potential difference between the ionic hydrogel electrode and ground increases. The change of the electric potential difference drives the electron flow in the external circuit. The generated current can essentially be described by time-variation of polarization field in the Maxwell's displacement current as proposed

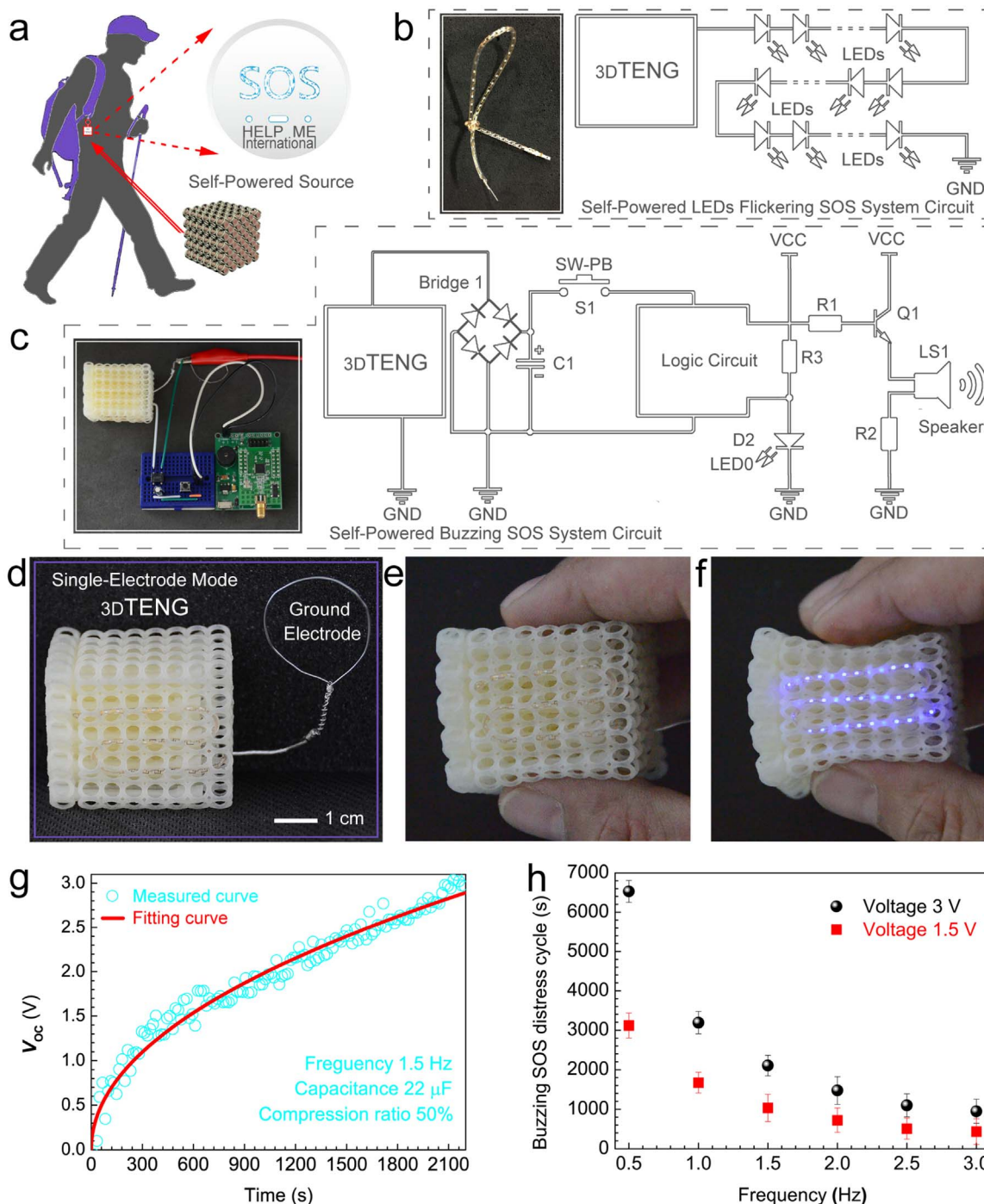


Fig. 5. Biomechanical energy harvesting by the ultraflexible 3D-TENG as a self-powered source. a, Illustration of an application as self-powered source for SOS distress signal system. b, Self-powered LEDs flickering SOS distress system circuit, transparent and flexible blue LEDs filament. c, Self-powered buzzing SOS distress system circuit and its digital photograph. d, Digital photograph of the ultraflexible self-powered LEDs flickering SOS distress device (sizes of 3.5 cm × 3.5 cm × 3.5 cm). e, Digital photographs of the device before compression and after compression (f). g, The voltage-time relationship at load capacitances of 22-μF. h, The relationship between working frequency and distress call cycle of self-powered buzzing SOS distress signal system with 1.5 V or 3 V operating voltage.

by Wang [43,44]:

$$J_D = \frac{\partial D}{\partial t} = \epsilon \frac{\partial E}{\partial t} + \frac{\partial P_S}{\partial t} \quad (1)$$

where J_D is the Maxwell's displacement current, D is the electric displacement field, E is the electric field, P_S is the polarization field induced by the surface polarization charges, ϵ is the permittivity of the dielectrics. The first term is the induced current by the varying electric field, and the second term is the current caused by the polarization field of surface electrostatic charges. The density $\sigma_1(z, t)$ of free electron accumulation in the metal electrode is a function of the gap distance z (t) between the two dielectrics. Thus, the Maxwell's displacement current can be expressed by

$$J_D = \frac{\partial D_z}{\partial t} = \frac{\partial \sigma_1(z, t)}{\partial t} = \sigma_c \frac{dz}{dt} \frac{d_1 \epsilon_0 / \epsilon_1 + d_2 \epsilon_0 / \epsilon_2}{[d_1 \epsilon_0 / \epsilon_1 + d_2 \epsilon_0 / \epsilon_2 + z]^2} + \frac{d\sigma_c}{dt} \frac{z}{d_1 \epsilon_0 / \epsilon_1 + d_2 \epsilon_0 / \epsilon_2 + z} \quad (2)$$

where σ_c is the triboelectricity introduced surface charge density, and the two dielectrics have the permittivities of ϵ_1 and ϵ_2 and thicknesses d_1 and d_2 , respectively. This equation means that the displacement current density is proportional to the charge density on the dielectric surface and the speed at which the two dielectrics contact/separate. In this entire cycle, this mode works in a way that relies on the charge exchange between the hydrogel electrode and ground, therefore, this is the electrical output characteristics of the ultraflexible 3D-TENG.

To measure the electrical output of the ultraflexible 3D-TENG, we printed a size of 3.5 cm × 3.5 cm × 3.5 cm (length × width × height) in the experiments. The frequency (~ 1.3 Hz) of the compression-recovery motion was controlled to be the same by a linear motor for all the tests. The peak voltage (V_{oc}) is in the order of ~ 62 V at open-circuit conditions (Fig. 2d). Under short-circuit conditions, the alternative volume current density (J_{sc}) was measured with a peak value of ~ 26 mA/m³ (Fig. 2e), and Fig. 2f shows the transferred volume charge density (ρ_{sc}) of ~ 0.65 mC/m³ in each cycle. By varying the external resistance, the maximum output power density (P_v) per unit volume was measured to be ~ 10.98 W/m³ at a matched resistance of ~ 0.75 teraohm (Fig. 2g).

3.2. Optimization of the ultraflexible 3D-TENG

Hybrid 3D printing of additive manufacturing technology enables the fabrication of such complex, multiscale structures of 3D-TENG for more efficient energy harvesting through computer-aided design (CAD) and optimization design of ink materials. Obviously, the effective contact area and the structure of electrification materials are the main factors which influence the output performance of ultraflexible 3D-TENG. A series of parameters with respect to the output performance were adjusted by 3D printing, and the corresponding V_{oc} , J_{sc} , and ρ_{sc} were measured at the same size (3.5 cm × 3.5 cm × 3.5 cm). The structure and parameters (D , r , h and d) of the ultraflexible 3D-TENG were shown Fig. 3a. The V_{oc} decreases with the increases of D and d , as shown in Fig. 3b and d, which is because that V_{oc} depends on the relative interval (h) between the resin I and resin II in the contact-separation motion. Provided that other conditions are invariant, as the D or d increases, the distance h decreases dramatically. However, the J_{sc} trend is exactly the opposite with the increases of D and d , due to the improvement in the effective contact area of electrification materials (Fig. 3b and d). Meanwhile, the ρ_{sc} increases with the increases of D and d because of the same principle, as shown in Fig. 3c and e. The larger the effective contact area (per unit volume), the more electrostatic charges generated at the interface and thus the higher J_{sc} and ρ_{sc} [45–53].

The compression ratio of the ultraflexible 3D-TENG was also varied to demonstrate its effect on the output performances. We used a programmable linear motor to control the compression ratio of each cycle

(Fig. 4a and b), and measured the electrical outputs under different compressing ratios. The results show that the output performances (V_{oc} , J_{sc} , ρ_{sc}) of the 3D-TENG are influenced by the compressing ratio (Fig. 4c), which is consistent with the Maxwell's displacement current equation. That is because increasing the compression ratio will improve the effective contact area of the 3D-TENG and increase the generated electrostatic charges per unit volume. And the influence of compression ratio on the peak power density P_v is similar (Fig. 4d). Subsequently, we double the size of the cubical 3D-TENG without changing the structure (length varies from 3.5 cm to 7.0 cm, Fig. 4e), and found that the V_{oc} increases with the equal proportion. But the J_{sc} and ρ_{sc} changes in the opposite trend because the increasing rate of effective contact area was lower than the increase of the volume (Fig. 4f). The high performance of the ultraflexible 3D-TENG indicates that it could efficiently harvest energy from various kinds of biomechanical motions.

One the other hand, one major concern about the hydrogel is the dehydration along with time, which can deteriorate its ionic conductivity and mechanical elasticity. When kept in an environment of an average relative humidity (RH) of ~ 35% at 20 °C, the long-term stability/reliability of the ultraflexible 3D-TENG was examined, as exhibited in Fig. 4g. It was found that there is a slight decrease of its electrical output response (less than 4.8% on average) after one week (over 800 cycles). However, after a month, the re-performed tests indicate there is no noticeable degradation, as confirmed by the remained output performance of ~ 56 V (V_{oc}), ~ 23.5 mA/m³ (J_{sc}) and ~ 0.59 mC/m³ (ρ_{sc}). The output performance of the 3D-TENG is affected by the PAAm-LiCl hydrogel electrode. When the PAAm-LiCl hydrogel loses water quickly for short time (in the first one week), the triboelectrification will be weakened with the decreased surface charges, and then can remain stable for long time. Whereas the dehydration is greatly alleviated when the PAAm-LiCl hydrogel is sealed with the resin part, the improved antidehydration capability is mainly because that the resin as external package can prevent the water evaporation [54–56]. Therefore, the steady and consistent electrical output was obtained despite the slight loss of water content after one month. This demonstrated antidehydration performance of the 3D-TENG ensures its applicability in many harsh environments.

3.3. Self-powered SOS flickering and buzzing distress signal system

On the basis of the strong advantages of the ultraflexible 3D-TENG demonstrated above, we develop a smart self-powered system to send out the SOS distress signal in the field (Fig. 5a), only relying on the weak stress from biomechanical motions. The system is comprised of a person, an ultraflexible 3D-TENG, simple management circuit, and some low-power electronics (such as LEDs and buzzer). Furthermore, the output of the 3D-TENG can be regulated to charge energy storage devices (capacitors or batteries) for powering different wearable electronics. The equivalent circuits of the self-powered LEDs flickering and buzzing SOS distress signal system are shown in Fig. 5B and C, respectively, including the illustrations for a transparent and flexible LEDs filament (Supplementary Fig. 6 and Supplementary Fig. 7) and the real circuit of device (Fig. 5c). A single-electrode mode 3D-TENG was used for self-powered source and pinched by the finger, where the filament with 40 blue light-emitting diodes (LEDs) connected in series can be easily lighted up (Fig. 5d, e and f). It can realize desired LEDs flickering SOS distress signal in the field by turning pinched frequencies of the fingers, especially at night (Supplementary Fig. 8 and Supplementary Video 2).

Supplementary material related to this article can be found online at <http://dx.doi.org/10.1016/j.nanoen.2017.12.049>

One the other hand, the self-powered buzzing SOS device could send distress calls just by pinched by the finger to charge a capacitor and to power an electronic buzzer. It was comprised of a 3D-TENG, a 3-V voltage electronic buzzer integrated circuit board, a diode-bridge (rectifying the alternating output signals), a 22-μF capacitor

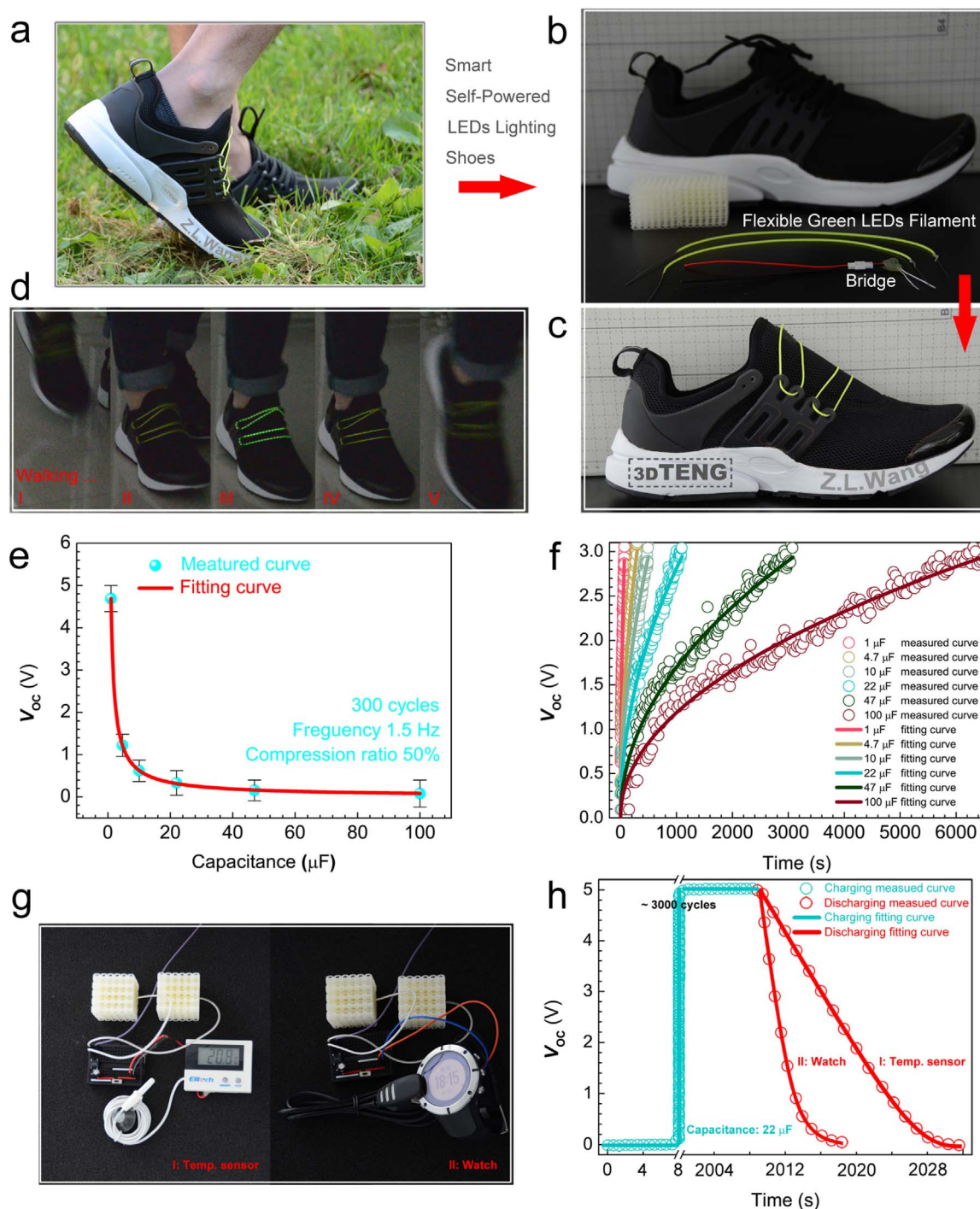


Fig. 6. A Portable self-powered system for driving and charging commercial electronics. a, Illustration of the ultraflexible 3D-TENG as the smart self-powered LEDs lighting shoes. b, Digital photographs of its components and after molding (c). d, Captured video snapshots of the self-powered LEDs lighting shoes while the wearer walks. e, The relationship between voltage and load capacitance at 300 working cycles. f, The *voltage-time* relationship at different load capacitances. g, Digital photographs of driving a smart temperature sensor and charging a battery of electronic watch. h, Voltage profile of a 22- μF capacitor being charged by the ultraflexible 3D-TENG and used to power temperature sensor (I) / charging a battery of electronic watch (II).

(accumulating charges), and a switch. The procedure of charging based on these circuits is presented in Fig. 5g. The device will emit persistent high decibel sound through buzzer when the capacitor reaches a pre-determined 3-V voltage, in which the threshold voltage can be adjusted based on different integrated circuits. Then, the relationship between the working frequency and distress call cycle of the self-powered buzzing SOS system with 1.5 V or 3 V threshold voltage is shown in Fig. 5H. When a user is helpless in the field (without food, no physical strength or even unable to move when running out of batteries), the

self-powered LEDs flickering or buzzing SOS devices emits its distress signals through weak human finger motions handily.

3.4. Ultraflexible 3D-TENG as a self-powered source

To make the ultraflexible 3D-TENG easier to drive or charge portable electronics, smart self-powered LEDs lighting shoes are developed (Fig. 6a and Supplementary Fig. 9). Fig. 6b shows all the necessary components in the smart lighting shoe, and its digital photograph after

formed is shown in Fig. 6c. All the components in this shoe are ultra-flexible, small-sized, and could be embedded in a specially designed insole without compromising the functionality and comfort for a person. A set of video snapshots of the smart self-powered LEDs lighting shoes are captured when the wearer walks, as shown in Fig. 6d (Supplementary Video. 3). Detailed instructions for assembling process and walking process are shown in Supplementary Fig. 9 and Supplementary Fig. 10. It is more important that the smart self-powered LEDs lighting shoes are able to offer security warning function at a trail running, climbing or night running, without any other power sources (for example, dry cell or lithium battery).

Supplementary material related to this article can be found online at <http://dx.doi.org/10.1016/j.nanoen.2017.12.049>

Finally, a portable self-powered system was also developed by integrating two 3D-TENGs with self-building converting/accumulating charge circuit core components for diode-bridge and capacitor. The viability of the charging electronics by biomechanical energy harvesting at compressed states was further evaluated. The relationship between charging voltage and load capacitance at 300 working cycles was measured, and then the charging *voltage-time* relationship at different load capacitances are shown in Fig. 6e and f, respectively. To demonstrate charging capability of the system as a practical power source, a self-powered temperature sensing system and a charging system for a battery of smart watch were developed, as shown in Fig. 6g. When the compression frequency of about 1.5 Hz was applied to the 3D-TENG, the charging voltage of the capacitors reaches a constant value of 5 V after ~ 3000 working cycles (Fig. 6h). It is clearly seen that the system can later power the temperature sensor for over 20 s (Fig. 6h and Supplementary Video. 4). The smart watch is charged by connecting the batteries with the self-powered system, and can be powered for about 7 s (Fig. 6g and h). Subsequently, the capacitor can be charged back to 5 V in about ~ 3000 working cycles and can power them repeatedly, where this charging cycle can be changed through adjusting the compression frequency and capacitance. Excellent performance of this system could be evidence for the 3D-TENG as a promising power source to be applied in self-powered electronic devices and their controlling. Based on the hybrid 3D printing, the 3D-TENG is ultraflexible, biocompatible and structure-adjustable, so it can provide a continuous uniform enough direct-current power to drive various commercial electronics or to charge the battery. It is capable of adapting to different deformations of supporting objects in any irregular shape and therefore has high potential in wearable electronics, smart robots and Internet of Things, etc. We believe that on the basis of the ultraflexible 3D-TENG, many kinds of application areas will spring out to make people's life more fascinating.

Supplementary material related to this article can be found online at <http://dx.doi.org/10.1016/j.nanoen.2017.12.049>

4. Conclusions

Nowadays, the rapid development of wearable electronics requires sustainable power sources. Here, for the first time, we have developed a hybrid 3D printing of ultraflexible TENG, which is soft, elastic, and able to be utilized to drive or charge commercial electronics, such as the self-powered LEDs flickering and buzzing SOS distress signal systems, as well as the smart self-powered LEDs lighting shoes. A portable self-powered temperature sensor or a smart watch is also successfully developed. The ultraflexible 3D-TENG and the new method of hybrid 3D printing are unique and distinct in its fundamental mechanism, which can effectively avoid problems that includes layer-by-layer structures, inconvenient fabrication process and inescapable elastic supporting for reciprocating motions. Additionally, this approach demonstrates complicated high-density integration while maintaining high flexibility. Considering the easy/exact controllability fabrication process (micron scale) and the common resin materials used, it could be able to achieve high flexibility, high precision, large area, and mass production in the

future. With the innovative fabrication technology, people can foresee great potential of 3D Printing-TENG-based portable self-powered sources in wearable devices, and potential applications in artificial intelligence and Internet of Things.

Acknowledgements

This study was supported by the “Thousands Talents” program for pioneer researcher and his innovation team, China, thanks for the support from “National Natural Science Foundation of China, China” (Grant nos. 61405131, 51432005, 5151101243, 51561145021, 51702018, 11704032), the National Key R & D Project from Minister of Science and Technology (2016YFA0202704), Beijing Municipal Science & Technology Commission (Y3993113DF, Z17110000317001).

Appendix A. Supporting information

Supplementary data associated with this article can be found in the online version at <http://dx.doi.org/10.1016/j.nanoen.2017.12.049>

References

- [1] Z.L. Wang, J. Song, *Science* 312 (2006) 242–246.
- [2] Z.L. Wang, *Adv. Funct. Mater.* 18 (2008) 3553–3567.
- [3] C. Keplinger, J.-Y. Sun, C.C. Foo, P. Rothemund, G.M. Whitesides, Z. Suo, *Science* 341 (2013) 984–987.
- [4] A. Chortos, J. Liu, Z. Bao, *Nat. Mater.* 15 (2016) 937–950.
- [5] J. Liang, L. Li, X. Niu, Z. Yu, Q. Pei, *Nat. Photonics* 7 (2013) 817–824.
- [6] K. Tian, J. Bae, S.E. Bakarich, C. Yang, R.D. Gately, G.M. Spinks, M. Panhuis, Z. Suo, J.J. Vlassak, *Adv. Mater.* 29 (2017) 1604827.
- [7] B. Tian, T. Cohen-Karni, Q. Qing, X. Duan, P. Xie, C.M. Lieber, *Science* 329 (2010) 830–834.
- [8] M.S. White, et al., *Ultrathin, highly flexible and stretchable PLEDs*, *Nat. Photonics* 7 (2013) 811–816.
- [9] C.B. Highley, C.B. Rodell, J.A. Burdick, *Adv. Mater.* 27 (2015) 5075–5079.
- [10] A.D. Valentine, T.A. Busbee, J.W. Boley, J.R. Raney, A. Chortos, A. Kotikian, J. Daniel Berrigan, M.F. Durstock, J.A. Lewis, *Adv. Mater.* 27 (2017) 1703817.
- [11] F.-R. Fan, Z.-Q. Tian, Z.L. Wang, *Nano Energy* 1 (2012) 328–334.
- [12] G. Zhu, J. Chen, T.J. Zhang, Q.S. Jing, Z.L. Wang, *Nat. Commun.* 5 (2014) 3426.
- [13] H. Wu, Y. Huang, F. Xu, Y. Duan, Z. Yin, *Adv. Mater.* 28 (2016) 9881–9919.
- [14] J. Chen, Y. Huang, N. Zhang, H. Zou, R. Liu, C. Tao, X. Fan, Z.L. Wang, *Nat. Energy* 1 (2016) 16138.
- [15] J. Chen, Z.L. Wang, *Joule* 1 (2017) 480–521.
- [16] Z.L. Wang, *ACS Nano* 7 (2013) 9533–9557.
- [17] U. Khan, S.-W. Kim, *ACS Nano* 10 (2016) 6429–6432.
- [18] X. Pu, W. Song, M. Liu, C. Sun, C. Du, C. Jiang, X. Huang, D. Zou, W. Hu, Z.L. Wang, *Adv. Energy Mater.* 6 (2016) 1601048.
- [19] Y. Yu, H. Sun, H. Orbay, F. Chen, C.G. England, W. Cai, X. Wang, *Nano Energy* 27 (2016) 275–281.
- [20] X. Pu, L. Li, M. Liu, C. Jiang, C. Du, Z. Zhao, W. Hu, Z.L. Wang, *Adv. Mater.* 28 (2016) 98–105.
- [21] Y.-C. Lai, J. Deng, S. Niu, W. Peng, C. Wu, R. Liu, Z. Wen, Z.L. Wang, *Adv. Mater.* 28 (2016) 10024–10032.
- [22] F. Yi, J. Wang, X. Wang, S. Niu, S. Li, Q. Liao, Y. Xu, Z. You, Y. Zhang, Z.L. Wang, *ACS Nano* 10 (2016) 6519–6525.
- [23] F. Yi, L. Lin, S. Niu, P.K. Yang, Z. Wang, J. Chen, Y. Zhou, Y. Zi, J. Wang, Q. Liao, Y. Zhang, Z.L. Wang, *Adv. Funct. Mater.* 25 (2015) 3688–3696.
- [24] B.-U. Hwang, J.-H. Lee, T.Q. Trung, E. Roh, D.-I. Kim, S.-W. Kim, N.-E. Lee, *ACS Nano* 9 (2015) 8801–8810.
- [25] K.N. Kim, J. Chun, J.W. Kim, K.Y. Lee, J.-U. Park, S.-W. Kim, Z.L. Wang, J.M. Baik, *ACS Nano* 9 (2015) 6394–6400.
- [26] X. Chen, X. Pu, T. Jiang, A. Yu, L. Xu, Z.L. Wang, *Adv. Funct. Mater.* 27 (2016) 1603788.
- [27] S.E. Bakarich, M. in het Panhuis, S. Beirne, G.G. Wallace, G.M. Spinks, *J. Mater. Chem. B* 1 (2013) 4939–4946.
- [28] B.W. An, K. Kim, H. Lee, S.-Y. Kim, Y. Shim, D.-Y. Lee, J.Y. Song, J.-U. Park, *Adv. Mater.* 27 (2015) 4322–4328.
- [29] A.D. Valentine, T.A. Busbee, J.W. Boley, J.R. Raney, A. Chortos, A. Kotikian, J.D. Berrigan, M.F. Durstock, J.A. Lewis, *Adv. Mater.* (2017) 1703817.
- [30] C.B. Highley, C.B. Rodell, J.A. Burdick, *Adv. Mater.* 27 (2015) 5075–5079.
- [31] S. Gong, W. Schwalb, Y. Wang, Y. Chen, Y. Tang, J. Si, B. Shirinzadeh, W. Cheng, *Nat. Commun.* 5 (2014) 3132–3139.
- [32] S. Niu, Z.L. Wang, *Nano Energy* 14 (2015) 161–192.
- [33] F. Yi, X. Wang, S. Niu, S. Li, Y. Yin, K. Dai, G. Zhang, L. Lin, Z. Wen, H. Guo, J. Wang, M.-H. Yeh, Y. Zi, Q. Liao, Z. You, Y. Zhang, Z.L. Wang, *Sci. Adv.* 2 (2016) e1501624.
- [34] J.-Y. Sun, X. Zhao, W.R.K. Illeperuma, O. Chaudhuri, K.H. Oh, D.J. Mooney, J.J. Vlassak, Z. Suo, *Nature* 489 (2012) 133–136.
- [35] C.H. Yang, B. Chen, J. Zhou, Y.M. Chen, Z. Suo, *Adv. Mater.* 28 (2016) 4480–4484.

- [36] F.-R. Fan, L. Lin, G. Zhu, W. Wu, R. Zhang, Z.L. Wang, *Nano Lett.* 12 (2012) 3109–3114.
- [37] S. Kim, M.K. Gupta, K.Y. Lee, A. Sohn, T.Y. Kim, K.-S. Shin, D. Kim, S.K. Kim, K.H. Lee, H.-J. Shin, D.-W. Kim, S.-W. Kim, *Adv. Mater.* 26 (2014) 3918–3925.
- [38] D.K. Davies, *J. Phys. D Appl. Phys.* 2 (1969) 1533.
- [39] R.G. Horn, D.T. Smith, *Science* 256 (1992) 362–364.
- [40] Q. Liang, X. Yan, Y. Gu, K. Zhang, M. Liang, S. Lu, X. Zheng, Y. Zhang, *Sci. Rep.* 5 (2015) 9080.
- [41] K.Y. Lee, M.K. Gupta, S.-W. Kim, *Nano Energy* 14 (2015) 139–160.
- [42] B. Chen, W. Tang, C. Zhang, L. Xu, L. Zhu, L. Yang, C. He, J. Chen, L. Liu, T. Zhou, Z.L. Wang, *Nano Res.* (2017), <http://dx.doi.org/10.1007/s12274-017-1716-y>.
- [43] Z.L. Wang, T. Jiang, L. Xu, *Nano Energy* 39 (2017) 9–23.
- [44] Z.L. Wang, *Mater. Today* 20 (2017) 74–82.
- [45] L. Pan, A. Chortos, G. Yu, Y. Wang, S. Isaacson, R. Allen, Y. Shi, R. Dauskardt, Z. Bao, *Nat. Commun.* 5 (2014) 3002.
- [46] J. Kim, M. Lee, H.J. Shim, R. Ghaffari, H.R. Cho, D. Son, Y.H. Jung, M. Soh, C. Choi, S. Jung, K. Chu, D. Jeon, S.-T. Lee, J.H. Kim, S.H. Choi, T. Hyeon, D.-H. Kim, *Nat. Commun.* 5 (2014) 5747.
- [47] S.W. Chen, X. Cao, N. Wang, L. Ma, H.R. Zhu, M. Willander, Y. Jie, Z.L. Wang, *Adv. Energy Mater.* 7 (2017) 1601255.
- [48] F. Yi, X. Wang, S. Niu, S. Li, Y. Yin, K. Dai, G. Zhang, L. Lin, Z. Wen, H. Guo, J. Wang, M.-H. Yeh, Y. Zi, Q. Liao, Z. You, Y. Zhang, Z.L. Wang, *Sci. Adv.* 2 (2016) e1501624.
- [49] J. Bae, J. Lee, S. Kim, J. Ha, B.-S. Lee, Y. Park, C. Choong, J.-B. Kim, Z.L. Wang, H.-Y. Kim, J.-J. Park, U.-I. Chung, *Nat. Commun.* 5 (2014) 4929.
- [50] F.R. Fan, W. Tang, Z.L. Wang, *Adv. Mater.* 28 (2016) 4283–4305.
- [51] S. Niu, Z.L. Wang, *Nano Energy* 14 (2015) 161–192.
- [52] X. Fan, J. Chen, J. Yang, P. Bai, Z. Li, Z.L. Wang, *ACS Nano* 9 (2015) 4236–4243.
- [53] C. He, C. Han, G. Gu, T. Jiang, B. Chen, Z. Gao, Z.L. Wang, *Adv. Energy Mater.* (2017) 1700644.
- [54] X. Pu, M. Liu, X. Chen, J. Sun, C. Du, Y. Zhang, J. Zhai, W. Hu, Z.L. Wang, *Sci. Adv.* (2017) e1700015.
- [55] H. Yuk, T. Zhang, G.A. Parada, X. Liu, X. Zhao, *Nat. Commun.* 7 (2016) 12028.
- [56] J.-Y. Sun, X. Zhao, W.R.K. Illeperuma, O. Chaudhuri, K.H. Oh, D.J. Mooney, J.J. Vlassak, Z. Suo, *Nature* 489 (2012) 133–136.